Maritime Moving Target Detection Technique for Passive Bistatic Radar with GNSS Transmitters

Fabrizio Santi[1], Debora Pastina[1], Marta Bucciarelli[2]

[1]Sapienza University of Rome
Department of Information Engineering, Electronics and Telecommunications
Via Eudossiana, 18, 00184 Rome, ITALY
santi@diet.uniroma1.it, debora@infocom.uniroma1.it

[2]Sympas s.r.l.
Viale Giulio Cesare, 71, 00192 Rome, ITALY
bucciarelli@sympas-srl.it

Abstract: *The paper puts forward a moving target detection technique for passive bistatic radar systems based on GNSS signals for maritime surveillance applications. If from one hand navigation satellites are extremely attractive as opportunistic sources for passive radar due to their global coverage and the availability of multiple satellites, on the other hand they provide a restricted power budget. To strengthen the target energy sufficiently to allow its detection, observation time has to be increased up to several tens of seconds. This requires the need to develop innovative techniques able to deal with such long integration times. In this paper, a local plane-based maritime moving target detection (M-MTD) technique is proposed. Such a technique performs the integration of the received signal for a long integration time, properly taking into account the migration of the moving target during the entire dwell time. Moreover, it provides target detection in the local plane that represents the section of maritime area covered by the radar antenna. Since this plane is common to multiple transmitters, the proposed technique can be easily extended to the multistatic case, which is the bigger benefit in using GNSS sources. Simulated and experimental results confirm the effectiveness of the proposed M-MTD technique to detect ship targets, not detectable with conventional MTD techniques, with the GNSS-based passive radar.*

1. Introduction

Global Navigation Satellite Systems (GNSS) signals are available over the entire Earth' surface. For this reason, alternative utilizations of these signals have been largely investigated. The analysis of the GNSS reflected signal (GNSS reflectometry) has brought to a number of well-established systems to remotely sense the atmosphere and ionosphere, ocean, land surface and cryosphere [1]. Moreover, as GNSS operate in the microwave region, innovative applications for passive radar systems have also begun to emerge [2]. In this field, navigation satellites have been employed in passive bistatic and multistatic synthetic aperture radar systems, providing a powerful tool for persistent local area monitoring [3-5]. Concerning the detection of moving targets, GNSS-based passive radar systems have been investigated for aerial target detection purposes [2,6-7].

In our research, we consider GNSS as illuminators of opportunity for an innovative passive radar system for maritime moving target detection. In the framework of maritime surveillance, passive radar systems have been intensively investigated over the last decade, since they allow low-cost and covert operation. Terrestrial sources such as DVB-T and GSM have been proved

being a suitable option to expensive and intrusive active systems for coastal surveillance purposes [8-9]. Nevertheless, they cannot provide radar coverage of open sea areas. Navigation satellites are one of the few choices to cope with the surveillance of maritime domain outside the territorial waters with passive coherent location (PCL) systems. Moreover, a single GNSS constellation guarantees that at the same time 6-8 satellites illuminate the same area. Therefore, a single sensor can simultaneously receive the signals from multiple sources, thus forming a multistatic radar system able to improve the system performance [10,11].

The major issue in using GNSS satellites as illuminators of opportunity is the very low level of electromagnetic filed reaching the Earth' surface [12]. This makes conventional techniques used for target detection inside terrestrial-based PCL systems not directly applicable to the GNSS-based passive radar. As well known, in conventional cases typical values of the integration times are in the order of hundreds of milliseconds. Due to the restricted power budget provided by the system under consideration, the integration time has to be increased remarkably to strengthen the received target energy sufficiently. Such long integration times imply the need to conceive, define and develop completely new techniques specifically tailored for the case of interest.

In this work, we introduce a new maritime moving target detection (M-MTD) technique able to integrate the signal reflections for long time intervals, in the order of several tens of seconds, thus allowing the retrieval of suitable values of signal-to-noise ratios (SNR) for the detection of ship targets. The developed technique works in a local plane representing the section of the maritime area covered by the radar antenna. The specific choice to work in the local plane instead of directly in the Range&Doppler (RD) plane (which is the common choice for conventional PCL systems) can be easily understood as follows. The bigger advantage of the GNSS sources is their inherent multistatic structure. Since the RD plane represents the point of view of the individual bistatic couple (i.e., transmitter-receiver), different RD planes have to be considered in the multistatic scenario, thus making challenging the combination of the multistatic detections. The local plane instead acts as common reference when multiple transmitters are involved, thus making the considered approach directly applicable to the multistatic scenario. As initial step, here we focus on the bistatic case and from the achieved results we outline some possible strategies to improve the system performance by exploiting multistatic acquisitions. The effectiveness of the proposed technique has been preliminarily investigated via simulations. Then, experimental results using GLONASS transmitter and a small fishing boat confirmed the capability of the proposed approach to enable M-MTD for the GNSS-based passive radar.

The remainder of the paper is organized as follows: Section 2 gives an overview of the GNSS-based passive radar and system geometry; Section 3 describes the proposed local plane-based M-MTD technique; simulated and experimental results are provided in Section 4 and Section 5, respectively, while some conclusions in Section 6 close the paper.

2. System Geometry and Operative Conditions

The operative conditions are given by a stationary sensor operating with two receiving channels. The former (referred to as Heterodyne Channel, HC) uses a low-gain antenna pointed toward the sky to record the direct signals from GNSS satellites, whereas the latter (Radar Channel, RC) employs a higher-gain antenna pointed toward the area to be surveyed collecting the signal reflections. Since GNSS operate on frequency or code division approaches, the receiver can separate the signals emitted by different sources, and each bistatic link can be processed separately. Hereinafter we consider a scenario comprising a single GNSS transmitter.

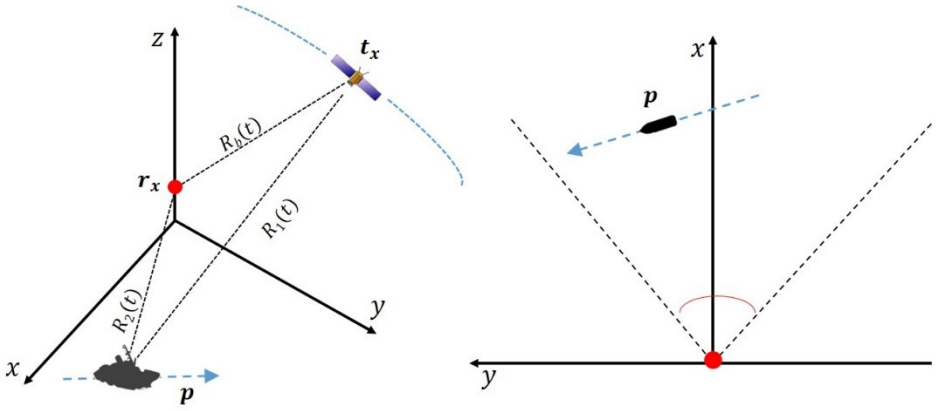

Figure 1. Local reference system – a) three-dimensional view, b) top-view.

Fig. 1 sketches the $(0, x, y, z)$ cartesian reference system, which is obtained as a rotation of the East-North-Up (ENU) reference system making the x-axis coinciding with the pointing direction of the radar antenna. Let $\boldsymbol{t_x}$, $\boldsymbol{r_x}$ and $\boldsymbol{p}$ denote the transmitter, receiver and target instantaneous positions, respectively. Without loss of generality, we assume that the origin of the reference system is the projection of the receiver position onto the ground plane (x, y). We assume a ship moving within the radar antenna footprint for the whole observation time T_{obs}. Moreover, to derive the mathematical model, the ship is modelled as single point-like target. We point out that this assumption is quite reasonable, due to the coarse resolution offered by the considered system.

Let t be the slow time defined in the interval $\left[-\frac{T_{obs}}{2}, \frac{T_{obs}}{2}\right]$, the instantaneous distances between satellite, receiver and target are defined as follows: $R_1(t) = |\boldsymbol{t_x} - \boldsymbol{p}|$ is the transmitter to target distance, $R_2(t) = |\boldsymbol{p} - \boldsymbol{r_x}|$ is the target to receiver distance and finally $R_b(t) = |\boldsymbol{t_x} - \boldsymbol{r_x}|$ is the transmitter to receiver baseline. Since range compression in the passive system is achieved by matched filtering with a reference signal compensating the instantaneous delay between transmitter and receiver, the bistatic range history of the target is given by

$$R(t) = R_1(t) + R_2(t) - R_b(t) \tag{1}$$

and its Doppler frequency is obtained as

$$f_d(t) = -\frac{1}{\lambda}\dot{R}(t) \tag{2}$$

being λ the wavelength of the transmitted signal and $\dot{R}(t)$ the first derivative of range with respect to time.

3. Maritime Moving Target Detection Technique

The goal of the developed M-MTD technique is to detect a moving target within the local plane and provide an estimation of its velocity by integrating the signal returns during an observation time long enough so that a sufficient SNR can be obtained. The proposed technique is composed by a cascade of three steps: pre-processing, RD maps formation, local maps formation. Fig. 2 shows the block diagram of the technique.

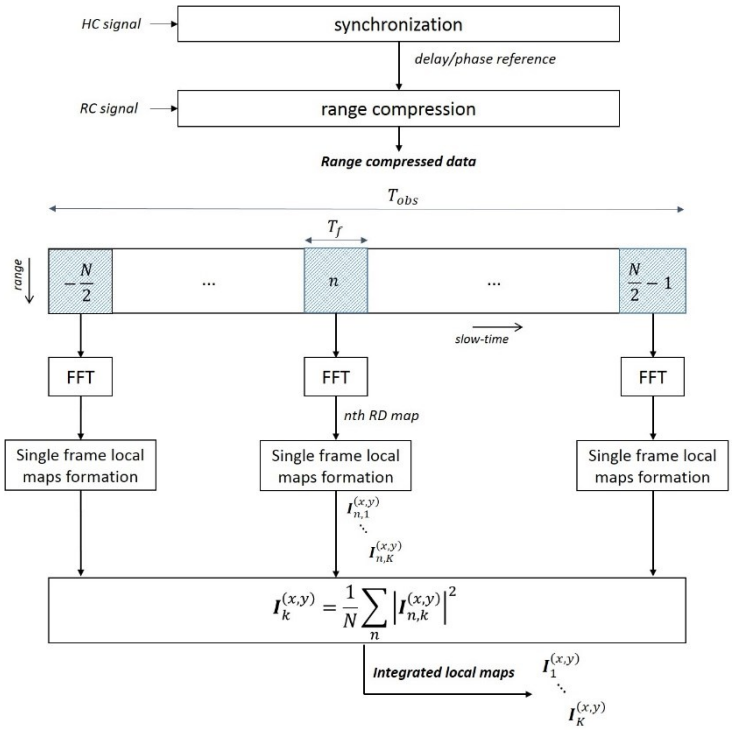

Figure 2. Block diagram of the local plane-based M-MTD technique.

3.1 Pre-processing

GNSS signals are continuous wave. Therefore, radar data reformatting according to an equivalent pulse repletion interval PRI (usually set equal to the duration of the transmitted code) is initially performed. Then, range-compression of the data received by the RC antenna is obtained by matched filtering with a noise-free replica of the transmitted signal, whose parameters, i.e. time-delay, Doppler frequency, phase and, if included, navigation message, are retrieved by tracking the direct signal parameters recorded by the HC [4] (synchronization step in Fig. 2).

At this point, range-compressed&slow-time data are divided into N consecutive slow-time frames of duration T_f. The single frame duration has to be set such that a coherence of the scattering mechanism can be assumed within each frame. In the considered maritime application, suitable values are in the order of 1-3 seconds.

3.2 Range&Doppler maps formation

Due to the limited duration of the single frames, target Doppler frequency can by assumed constant at the single frame level. Therefore, by performing a slow time FFT to each frame, N RD maps are obtained.

3.3 Local maps formation

While target position can be considered fixed at the single RD map level due to the coarse resolution and short integration time, the same does not apply when multiple maps are considered. The moving target changes its position during the observation time, thus giving rise to both range and Doppler migration. The range and Doppler position over which the target is located at the nth frame time t_n ($n = -N/2,\ldots, N/2-1$), i.e. $[R(t_n), f_d(t_n)]$ in (1) and (2),

```
for each frame
    for each target starting position under test
        for each target velocity under test
            calculate corresponding range position for t = t_n
            calculate corresponding Doppler position for t = t_n
            store corresponding value of the nth RD map in the matrix I_n
        end
    end
end
```

Figure 3. Pseudo-code of the single frame local maps formation process.

depends on its velocity $\boldsymbol{v} = \dot{\boldsymbol{p}}(t = t_0) = [v_x, v_y]$ as well as its position at the reference time $\boldsymbol{p}(t = t_0) = \boldsymbol{p}_0 = [x_0, y_0]$. Namely, the target trajectory corresponds to a range and Doppler history that has to be tracked along the RD maps, with the ultimate goal to integrate the signal returns over the entire dwell time. According to a specific quartic (x_0, y_0, v_x, v_y) under test, the RD position pertaining the nth frame is evaluated and the corresponding value of the RD map is stored in a four-dimension matrix $\boldsymbol{I}_n$. When all the possible position&velocity couples have been tested, for each frame a set of single frame local (x, y) maps $\boldsymbol{I}_{n,k}^{(x,y)}$ are obtained, being $k = 1, \dots, K$ the index of the tested velocities. For sake of clearness, Fig. 3 shows the pseudo-code accomplishing this procedure.

Obviously, the searching grids on both the space and velocity domains have to be properly set. The bounds of the searching grids on (x_0, y_0) define the surveyed area. Their sampling should be at least equal to the best range and azimuth resolutions provided by the system. Because of the best resolution values are obtained for the pseudo-monostatic geometry, the sampling along the x direction has to be set at least equal to the bistatic range resolution, while the sampling along the y direction should be set according to the best azimuth resolution. The bounds of the searching grids over the possible target velocities should be set according to the maximum possible target speed. In particular, the searching grid on v_x should span over the possible target radial velocities, with a sampling that has to assure a range variation from the reference at the last frame less than half range resolution cell. The grid over v_y defines the set of possible target tangential velocities, with a sampling that has to assure a Doppler variation from the reference at the last frame less than half Doppler resolution cell.

At the end of the procedure in Fig. 3, integration over the whole observation time has to be carried out. Assuming a target moving approximately with linear motion, the integration can be driven by the velocity value, by operating a quadratic integration of the N integrated maps $\boldsymbol{I}_{n,k}^{(x,y)}$ pertaining the same velocity, i.e.,

$$\boldsymbol{I}_{k}^{(x,y)} = \frac{1}{N}\sum_{n=-\frac{N}{2}}^{\frac{N}{2}-1}\left|\boldsymbol{I}_{n,k}^{(x,y)}\right|^2 \tag{3}$$

At this point, the presence of possible movers can be sought in the $\boldsymbol{I}_{k}^{(x,y)}$ maps, where the targets are likely isolated from the background and therefore detectable.

4. Simulated Results

The effectiveness of the proposed technique is shown in this section via simulations. The C/A code transmitted on the L1 band of a GPS satellite has been considered as opportunistic signal. Parameters of the simulated scenario are listed in Table I.

TABLE I. SIMULATED SCENARIO PARAMETERS

Parameter	value	unit
Constellation	GPS	-
SVID	15	-
Carrier frequency (L1 band)	1575.42	MHz
Chip-rate (C/A code)	1.023	MHz
Equivalent PRI (also code length)	1	ms
Transmitter position at reference time	[-719.36807, 5471.0844, 19656.66888]	km
Receiver position	[0, 0, 0]	km
Target position at reference time	[1300, 0, 0]	m
Target velocity	[0 5 0]	kn
Target radar cross section	25	dB

The observation time is set equal to 30 s and the range-compressed data are segmented in 30 consecutive frames 1 s long each. An additive white Gaussian noise occupying the useful signal bandwidth has been considered as disturbance background, which results in a SNR after matched filtering for range compression equal to -24 dB. Therefore, the coherent integration gain provided by the FFT carries to a SNR equal to 6 dB in the individual RD maps, which does not suffice for the target detection, taking into account the great fluctuations of the noise disturbance that makes difficult the application of autogates to extract the target position information. Fig. 4a shows the RD map corresponding to the central frame (normalized to the mean noise power), where we can observe that the target is buried in the noise. For comparison, Fig. 4b shows the corresponding noise-free case.

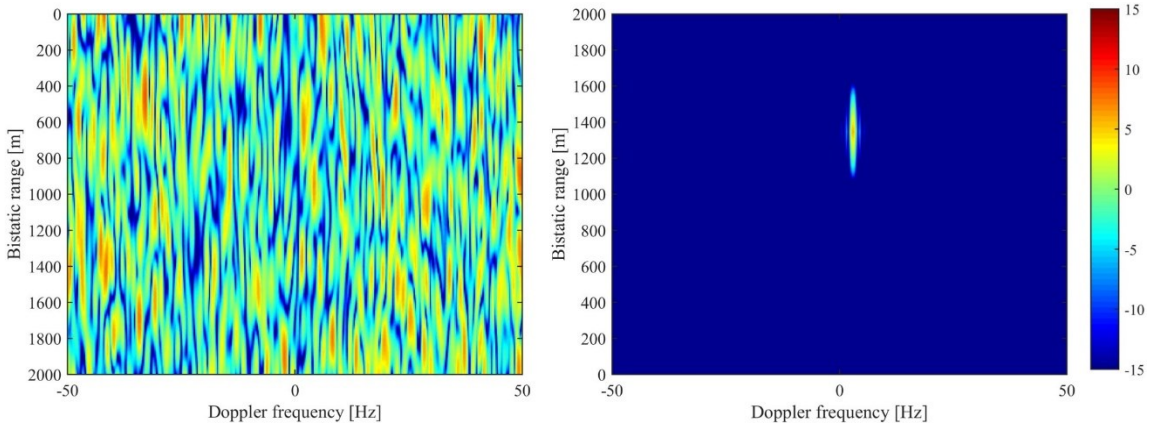

Figure 4. Single frame Range&Doppler map – a) with noise, b) noise-free.

By applying the proposed M-MTD technique, the noise fluctuations can be reduced by means of the non-coherent integration (3), whereas the target energy can be correctly collected over the different frames. Fig. 5 shows the local map resulting from the integration of the 30 single-frame maps pertaining the actual target velocity. In the map, 0 dB represents the mean noise power and we can observe that a bright spot is well visible around the actual target location.

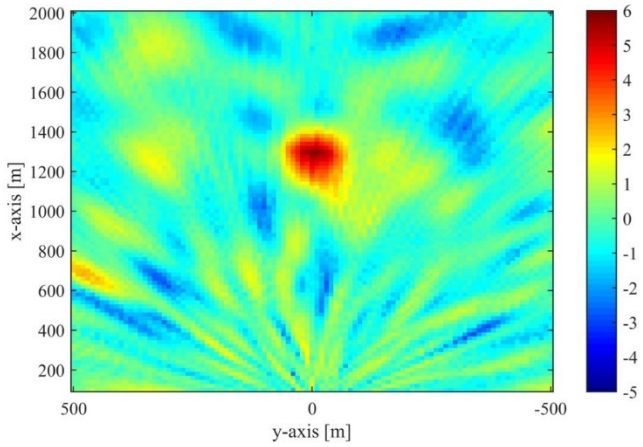

Figure 5. Integrated local map for the actual target velocity case.

Nevertheless, since the target velocity is generally unknown, all the maps corresponding to the tested velocities have to be screened. Fig. 6 shows the maps obtained for some velocities different from the actual value. As for Fig. 5, these maps have been normalized to mean noise power. We can observe that also for these velocities bright spots can be revealed in positions that differ from the actual target location. Despite considering a target velocity different from the actual value entails a lower coherent integration gain at the single frame level (i.e., a defocusing effect) and therefore a lower intensity in the final map, the peak intensities of the considered cases are sufficiently higher than the noise floor to be detected. The proposed technique ultimately suffers for an ambiguity problem between position and velocity, since more couples position&velocity of the target will be detected (indeed, different starting position&velocity may give rise to the same RD history). Therefore, the target can be detected in a ring of (x, y) positions and in a range of possible velocities.

However, it is easy to see that such ambiguities locate on iso-range contour. In Fig. 6, we can observe that the spots due to false target velocities are confined in the area defined the black dashed lines representing iso-ranges. It is worth to note that the orientation of the iso-ranges depends on the particular bistatic geometry. Therefore, when multiple satellites are involved, the different bistatic links give rise to different positions of the wrong detections, thus enabling their rejection. Obviously, such a rejection capability depends on the difference among the bistatic iso-ranges, which, from (1), will be greater for targets at higher ranges.

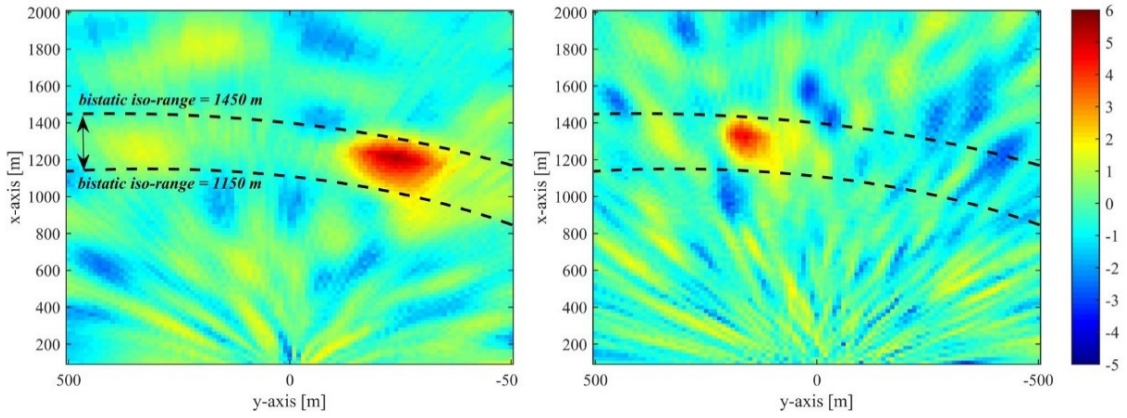

Figure 6. Integrated local maps for tested $\boldsymbol{v} = [0,3]$ kn (a) and $\boldsymbol{v} = [0,8.8]$ kn (b).

5. Experimental Results

An experimental campaign was conducted by the Microwave Integrated Systems Laboratory team of the University of Birmingham (UK) in the framework of the EU h2020 project "SpyGLASS" [13]. The experimental campaign is detailed in Fig. 7. The receiver prototype was located at the coastal area of the Aberystwyth in UK and GLONASS transmitters have been exploited. A fishing boat of approximately 10 m length was employed as target of opportunity and its real track was recorded by a GPS receiver. The ship was moving toward the receiver during the acquisition time, with approximately constant velocity $v_x = -3$ m/s and $v_y = -0.5$ m/s. Table II lists the parameters of the experiment.

(a) (b) (c)

Figure 7. Experimental campaign – a) target of opportunity, b) receiving hardware, c) acquisition geometry.

TABLE II. EXPERIMANTAL AND SIGNAL PROCESSING PARAMETERS

Parameter	value	unit
Constellation	GLONASS	-
SVID	732	-
Carrier frequency (L1 band)	1603.6875	MHz
Chip-rate (P-code)	5.110	MHz
Satellite elevation	73.2 – 73.1	deg
Satellite azimuth (clockwise from N)	3.0 – 6.8	deg
RC antenna pointing direction (clockwise from N)	280	deg
Equivalent PRI	1	ms
Sampling frequency	50	MHz
Observation time	118	s

After range compression, data are segmented in frames 1 s long each. Due to the small size of the target, the integrated target energy over a single RD map does not suffice to bring it out to the disturbance background, as it is apparent looking at the RD map pertaining the central frame of the acquisition shown in Fig. 8. In the figure, normalized to the mean disturbance power, the black star marker denotes the actual RD target position and we can observe that not any spot in the neighborhood can be identified as moving target.

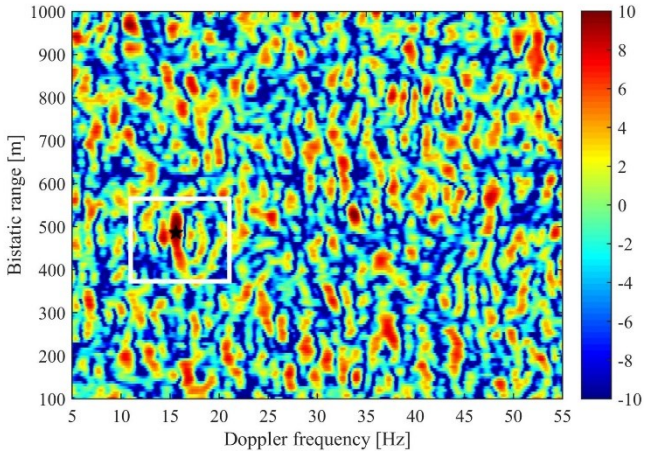

Figure 8. Central frame RD map.

The acquisition has been divided in three parts, where the first part refers to the observation time interval [0, 59]s, the second part to the interval [30-89]s and the third part to the interval [59,118]s. Fig. 9 shows the corresponding integrated maps over each 59 s long acquisition interval for the actual velocity recorded by the GPS receiver. In each map, 0 dB represents the mean disturbance power. The black star markers denote the target actual positions. We can observe that a bright spot appears in each map in a position corresponding to the actual target location. It is also interesting to note that better signal to disturbance ratios are achieved for increasing starting times of the considered dwell intervals. This is well in line with the fact that the target is moving toward the receiver during the acquisitions, thus furtherly confirming the capability of the proposed technique to enable M-MTD capability for the GNSS-based passive radar.

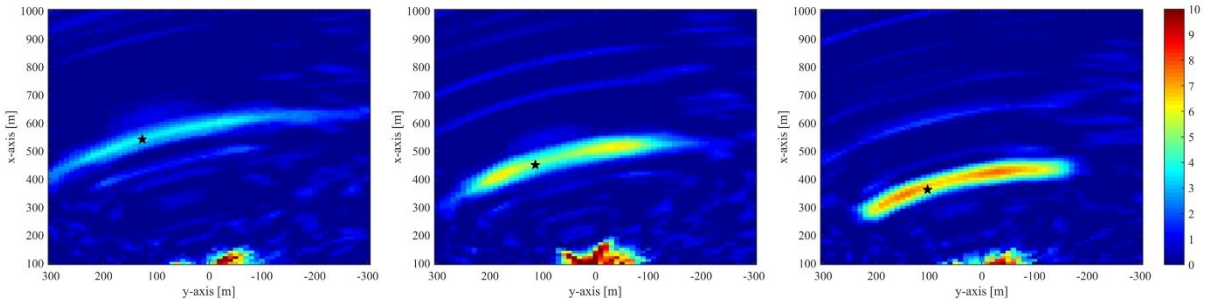

(a) (b) (c)

Figure 9. Experimental results – a) dwell interval [0-59]s, b) dwell interval [30-89]s, c) dwell interval [59-118]s.

6. Conclusions and Future Works

Our research considers GNSS as opportunity transmitters for passive bistatic radar aiming at maritime surveillance. The global coverage offered by GNSS satellites makes them extremely appealing for this kind of application. Nevertheless, they irradiate a very low power, thus making difficult the detection of the ship targets of interest. An innovative Maritime-Moving Target Detection technique has been proposed in this paper, able to strengthen the target energy sufficiently for MTD purposes by exploiting long integration times. Simulated and experimental results confirmed the effectiveness of the proposed technique to enable M-MTD capability for the GNSS-based passive radar. Moreover, the technique provides the detections in a plane that is common to different transmitters. Therefore, it allows a straightforward

extension of the approach to case of multiple satellites, which is one of the main benefits arising from the choice of GNSS as opportunistic sources, and it will be the focus of future steps of our research.

Acknowledgement

This project has received funding from the European GNSS Agency under the European Union's Horizon 2020 research and innovation programme under grant agreement No 641486, "GALILEO-BASED PASSIVE RADAR SYSTEM FOR MARITIME SURVEILLANCE — SpyGLASS".
The authors would like to thank Prof. M. Cherniakov and Dr. M. Antoniou of the University of Birmingham (UK) for providing the experimental data.

References

[1] S. Jin, G. P. Feng, and S. Gleason, "Remote sensing using GNSS signals: Current status and future directions," *Adv. Space Res.*, vol. 47, no. 10, pp. 1645-1653, May 2011.

[2] V. Koch and R. Westphal, "New approach to a multistatic passive radar sensor for air/space defense," *IEEE Aerosp. Electron. Syst. Mag*., vol. 10, no. 11, pp. 24-32, Nov. 1995.

[3] M. Cherniakov and T. Zeng, *Passive Bistatic SAR with GNSS Transmitters*, in *Bistatic Radar: Emerging Technology*, M. Cherniakov, Ed. New York: Wiley, 2008.

[4] M Antoniou and M. Cherniakov, "GNSS-based bistatic SAR: a signal processing view," *EURASIP J. Adv. Sign. Process*., 2013:98.

[5] F. Santi, D. Pastina, M. Bucciarelli, M. Antoniou, D. Tzagkas, M. Cherniakov, "Passive multistatic SAR with GNSS transmitters: Preliminary experimental study," *2014 11th European Radar Conference*, Rome, Oct. 2014, pp. 129-132.

[6] I. Suberviola, I. Mayordomo, and J. Mendizabal, "Experimental results of air target detection with a GPS forward-scattering radar," *IEEE Geosci. Remote Sens. Lett*., vol. 9, no. 1, pp. 47-51, Jan. 2012

[7] S. Wachtl, V. Koch, L.-P. Schmidt, "Global Navigation Satellite Systems in Passive Surveillance Applications," *Tyrrhenian International Workshop on Digital Communications – Enhanced Surveillance of Aircraft and Vehicles*, Rome, 2014, pp. 135-140.

[8] D. Langellotti, F. Colone, E. Tilli, A. Di Lallo, "Multi-frequency target detection techniques for DVB-T based passive radar sensors," *2014 IEEE Radar Conference*, Cincinnati, OH, USA, 19-23 May 2014.

[9] R. Zemmari, M. Daun, M. Feldmann, and U. Nickel, "Maritime surveillance with GSM passive radar: Detection and tracking of small agile targets," *Proc. of 14th Int. Radar Symp*., Dresden, 2013, pp. 245-251.

[10] F. Santi, M. Antoniou, and D. Pastina, "Point Spread Function Analysis for GNSS-Based Multistatic SAR," *IEEE Geosci. Remote Sens. Lett*., vol. 12, no. 2, pp. 304-308, Feb. 2015.

[11] F. Santi, M. Bucciarelli, D. Pastina, M. Antoniou, and M. Cherniakov, "Spatial Resolution Improvement in GNSS-Based SAR Using Multistatic Acquisitions and Feature Extraction," *IEEE Trans. Geosci. Remote Sens.*, vol. 54, no. 10, pp. 6217-6231, Oct. 2016.

[12] X. He, M. Cherniakov, and T. Zeng, "Signal detectability in SS-BSAR with GNSS non-cooperative transmitter," *IEE Proc. Radar Sonar Navig.*, vol. 152, no. 3, pp. 124-132, Jun. 2005.

[13] http://www.spyglassproject.eu